OAK RIDGE NATIONAL LABORATORY

MANAGED BY UT-BATTELLE, LLC.
POST OFFICE BOX 2008, OAK RIDGE, TENNESSEE 37831-6079

ORNL
CENTRAL FILES NUMBER

ORNL/CF-00/28

DATE: August 24, 2000

SUBJECT: Quarterly Technical Progress Report of the Radioisotope Power System Materials Production and Technology Program Tasks for April through June 2000

TO: Distribution

FROM: J. P. Moore

The enclosed revised report covers the third quarter of FY 2000. This report is one of a series to inform the Office of Space and Defense Power Systems, U.S. Department of Energy, and their contractors of accomplishments by the Oak Ridge National Laboratory which is operated by UT-Battelle. If you have any questions or require further clarification on any topic, please contact us at Building 4508, Mail Stop 6079.

JPM:smw

UCN-2383
(3 6-88)

QUARTERLY TECHNICAL PROGRESS REPORT OF RADIOISOTOPE POWER SYSTEM MATERIALS PRODUCTION AND TECHNOLOGY PROGRAM TASKS FOR APRIL THROUGH JUNE 2000

Prepared for Department of Energy
Office of Space and Defense Power Systems
under Budget and Reporting Classification
AF 70 10 20 0, AF 70 60 00 0, and AF 70 30 00 0

by

Radioisotope Power System Program
Metals and Ceramics Division
Oak Ridge National Laboratory

Oak Ridge National Laboratory
Oak Ridge, Tennessee 37831-6080
operated by UT-Battelle, LLC
for the
U.S. Department of Energy
Contract DE-AC05-00OR22725

This page intentionally blank

CONTENTS

1. INTRODUCTION

The Office of Space and Defense Power Systems (OSDPS) of the Department of Energy (DOE) provides Radioisotope Power Systems (RPS) for applications where conventional power systems are not feasible. For example, radioisotope thermoelectric generators were supplied by the DOE to the National Aeronautics and Space Administration for deep space missions including the Cassini Mission launched in October of 1997 to study the planet Saturn. The Oak Ridge National Laboratory (ORNL) has been involved in developing materials and technology and producing components for the DOE for more than three decades. For the Cassini Mission, for example, ORNL was involved in the production of carbon-bonded carbon fiber (CBCF) insulator sets, iridium alloy blanks and foil, and clad vent sets (CVSs) and weld shields (WSs).

This quarterly report has been divided into three sections to reflect program guidance from OSDPS for fiscal year (FY) 2000. The first section deals primarily with maintenance of the capability to produce flight quality carbon-bonded carbon fiber (CBCF) insulator sets, iridium alloy blanks and foil, clad vent sets (CVSs), and weld shields (WSs). In all three cases, production maintenance is assured by the manufacture of limited quantities of flight quality (FQ) components. The second section deals with several technology activities to improve the manufacturing processes, characterize materials, or to develop technologies for two new RPS. The last section is dedicated to studies of the potential for the production of 238Pu at ORNL.

2. PRODUCTION TASKS

2.1 CARBON-BONDED CARBON FIBER

The goal of this effort is to maintain production capability for CBCF insulation sets. These are produced under closely controlled conditions and stringent QA procedures to ensure compliance with material specifications at each step in the production process, from the handling of raw materials to shipment of finished parts. Dedicated facilities for CBCF production remain in the Carbon and Insulation Materials Technology Laboratory. Periodic exercise of production activities is performed to assure that the processes can be successfully executed and to verify personnel competencies, and adequacy of training, equipment, and procedures.

Our goals this year include (1) complete the fabrication and characterization of CBCF sleeves initiated in FY 1999; (2) produce and certify nine new sets of flight-quality CBCF sleeves and disks; (3) initiate the qualification of a new, commercially available resin by producing nine sets of sleeves and disks to the current flight-quality specification; (4) consolidate the storage of CBCF raw materials, archive specimens, and completed sets into a room designated the CBCF Laboratory to allow for greater control and exclusive use of facilities; and (5) initiate preparation of a comprehensive video of all CBCF production and qualification tasks.

2.1.1 CBCF Production Activities

Eighteen CBCF sleeves were machined from two molding runs that used the qualified resin (Durez 22352). All eighteen sleeves met flight quality dimensional requirements. Two CBCF disks were machined for each of eighteen sleeves from a plate molded in the current FY using Durez 22352 resin. Analytical and mechanical properties samples have been machined.

One molding run of CBCF sleeves was made using the new commercial resin (Oxychem Durez 5034). Nine CBCF sleeves were machined to flight quality dimensional requirements. The molding and machining characteristics of CBCF produced with Oxychem Durez 5034 resin was indistinguishable from the qualified resin. The 100% yield in CBCF sleeves with respect to dimensional requirements are attributed to the extraordinary machinist skill. The balance of qualification activities (i.e., x-ray and chemistry) will be carried out concurrently or consecutively to minimize set-up time and average cost of each component. The expected production for this year includes twenty-three flight quality CBCF insulator sets; five completed from FY 1999 efforts and eighteen produced in the current FY.

2.1.2 Inventory of Critical Materials (updated June 2000)

Carbonization run #52 was completed and yielded 800 gm of production-ready, carbonized fiber. Microfibers, Inc. was identified as a vendor to chop additional quantities of rayon for CBCF production. They have been previously used to accomplish this task in support of CBCF production.

The inventory of critical materials required for CBCF production was updated. Raw materials on hand include:

1. Chopped and carbonized rayon fiber: 16.3 kg., sufficient for 8 molding runs;
2. Chopped rayon fiber: 21 kg., sufficient for 11 molding runs after carbonization;
3. Unchopped rayon tow: 923 kg., sufficient for 450 molding runs after chopping and carbonization;
4. Phenolic resin (Durez 22352): 7 kg., sufficient for 23 molding runs.

2.1.3 Videotaping of CBCF Production and Qualification Tasks

Production of CBCF components is both an art and a science. Much of the science is specified in very detailed procedures that are followed for each step in the production and qualification of CBCF sleeves and disks. However, much of the art of handling this fragile material is not fully communicated in these procedures. To capture this art, a digital video of each step in fabrication and qualification is being made. A comprehensive video record will be completed in FY 2001 to serve as an archive of best practices and a back-up to the few skilled in the art.

2.2 IRIDIUM-ALLOY BLANK AND FOIL PRODUCTION

The goals for this activity are to produce flight-quality blanks and foil under full configuration control and to supply materials needed for clad vent set demonstration and maintenance activities. During the second quarter of FY 2000, iridium powder processing and electron beam melting of Ir-0.3% W was performed for the G3 ingot, and 69 blanks from 10 sheets from the G2 ingot were machined.

2.2.1 Blank Fabrication from G2 Ingot

Grinding and dimensional inspection of a total of 69 blanks from ten sheets from the G2 ingot were completed. A total of 66 passed the dimensional inspection. One blank was rejected because it had less than the minimum diameter. This was caused by slippage of the blank in the holder during electrodischarge machining. Two blanks did not clean up during grinding. The blanks were sampled and cleaned. Ultrasonic inspection of the 66 blanks resulted in 65 acceptable blanks and one blank rejected because of a small indication of an internal defect. All of the 65 blanks also passed dye-penetrant inspection. Visual inspection resulted in 59 prime blanks and 6 blanks to be reworked for surface defects. Metallographic inspection requirements for all blanks were satisfactorily completed. Chemical analysis requirements for bulk and surface analysis by glow discharge mass spectrography were performed using the Kratos instrument at the Y-12 Plant. Carbon and oxygen contents by combustion methods were also performed. All chemical analyses were within specification limits. The blanks should provide 40 blanks during FY 2000 and additional blanks during FY 2001.

2.2.2 Blank Fabrication from G3 Ingot

Powder processing was continued for the G3 ingot using 17.4 kg of blended iridium powder. The processing, which includes blending with tungsten powder, compacting, sintering and electron beam melting, was completed for four of the total of six batch blends for the G3 ingot. The G3 ingot should yield 90 blanks during FY 2001.

2.2.3 Arc Melting of Scrap Iridium Ingot

Arc melting of the RS14 iridium alloy scrap electrode using an improved pad design was successfully completed. The modified pad, to which the arc is initially struck from the electrode at the bottom of the water-cooled copper mold, was mechanically fixed to the bottom of the mold to avoid welding of the electrode to the pad. Welding of the pad to the electrode has occurred occasionally during the melting of iridium and other materials and requires that the melt be discontinued immediately. A similar redesigned pad had been used for melting of a number of other refractory metals with good success in the same furnace. The arc melting of the RS14 ingot with the redesigned pad resulted in improved vacuum levels during melting and improved ingot surface finish. The same iridium pad is planned for use in melting of the G3 ingot during the fourth quarter of FY2000.

2.2.4 Foil Production

A total of 11 pieces of foil from ingot GFR222, previously in storage, were transferred to the CVS task with an approved data package on May 16, 2000. A total of 18 pieces of stress-relieved foil, which had been certified to specification GPHS-M-186 Rev. D and placed in storage, was recrystallized. The processing was performed under SIDR Ir-79 to permit the foil to be upgraded to the current Rev. E of the foil specification. Metallographic examination of foil samples showed that the foil met recrystallization and grain size requirements. A new data package will be prepared for the foil.

2.3 CLAD VENT SETS AND WELD SHIELD

The goal of this activity is to produce flight quality (FQ) CVS and weld shields (WS) for inventory, test hardware and to maintain the production capability.

2.3.1 Training for FQ Production

Personnel retirements at the end of 1999 dictated the need for training in various operations, including dimensional inspection, frit vent manufacturing, cup forming and heat treatment for cup recrystallization, assembly air burn-off, and vacuum outgassing. One machinist was trained earlier for dimensional inspection. Training continues for the frit vent assembly operations as well as for cup forming and heat treatment.

Fifty-seven frit vent assemblies have been made since February 2000. Only 8 frit vent assemblies have had low flow rates or excessive thicknesses. This translates to a yield of 86%.

Non-flight quality blanks were made into blank assemblies, formed into cups, chemically stripped and cleaned and then vacuum heat treated. The cups were to be sized and processed further so that they could be used for weld shield tab-to-cup weld training. Unfortunately, none of the eleven cups would fit into the sizing die because their diameters were too large. Upon further review, it appears that the selected non-flight quality blanks D1-3-3, -4, -5, and -6 from the 2" diameter ingot process plus E1-2, -3, -4, -5 and E2-1, -3, -4 experimental test blanks from the old drop cast ingot process are responsible for the large as-formed diameters.

Twelve additional blanks (from current process 2.5" diameter ingots RS10 and RS11) have been scribed and are ready for acid cleaning before being welded into blank assemblies and formed into cups. As long as these cups can be properly sized, 15 already-scribed FQ blanks will be processed to finished cups. The requirement is to yield 5 FQ CVSs by the end of FY2000.

2.4 IRIDIUM POWDER AND INVENTORY MANAGEMENT

The purpose of this work is to manage an iridium inventory for all heat source contractors with emphasis on the significant quantities of iridium located at Babcock and Wilcox of Oho, Inc. (Mound Plant), Los Alamos National Laboratory (LANL), and Oak Ridge National Laboratory (ORNL), and to maintain a no-change iridium inventory through an annual write-off of inventory and processing losses.

2.4.1 Iridium Demand and Supply Schedule

The draft of the annual update of the Iridium Demand and Supply Schedule was completed in June. This annual update will be issued in July 2000.

2.4.2 Annual Write-Off Activity

The annual Fiscal Year 2000 write-off of iridium inventory was completed in May. A total of 1.2 kg of iridium was written off as a normal operating loss. The non-fund iridium inventory of the Office of Space and Defense Power Systems was decreased by 1.2 kg to reflect the loss, which was consistent with expectations.

2.4.3 Iridium Accountability Reviews

A review at Mound Plant was conducted on June 28 and 29, 2000. The purpose of this review was to evaluate the accountability, physical inventory, and security of iridium. It was concluded that the accountability for the iridium was in place and operating in a proper manner. No recommendations were necessary.

2.5 SHIELD CUP MODIFICATION

The goal of this activity is to widen the vent notches and install the integral weld shield (IWS) in 59 FQ and 9 EU shield cups returned from Los Alamos National Laboratory (LANL).

2.5.1 Establishing Capability for Installing IWS

Deviation requests for all of the procedures (and tooling drawings) for fabricating, inspecting, welding, assembling, and packing/shipping integral weld shields, shield cup assemblies, and matched assemblies were submitted and approved. The deviation requests and the applicable procedure(s) are listed:

DR-CVS-015 for GPHS-K-3620, Rev. B weld shield butt welding procedure;
DR-CVS-017 for GPHS-XF-3620, Rev. D weld shield fabrication and gphs-c-3620, rev. f weld shield inspection procedures;
DR-CVS-018 for GPHS-K-9754, Rev. C weld shield tab-to-shield cup welding procedure;
DR-CVS-019 for GPHS-G-9754, Rev. J shield cup assembly and GPHS-G-9808, Rev. T matched assembly procedures, and
DR-CVS-020 for GPHS-C-9754, Rev. E shield cup assembly inspection procedure.

It should be noted that the weld shield blanking punch was remade because the original developed a chipped corner that was being reproduced in the blanks. New butt weld hold-down clamps to permit sufficient clearance for the electron beam during welding were fabricated. The weld shield tab-to-shield cup weld fixture was successfully re-fabricated. A second and maybe a third copy will be required for production. Tantalum stock has been received in preparation for this eventuality.

Cracks were found in the weld shield butt welds after forming. Two subsequent changes were made as part of a successful effort to minimize the frequency of cracking during forming. The order of the butt-weld tab removal and forming steps was reversed so that the forming step is done before the butt-weld tab removal step. Procedure GPHS-XF-3620, Rev. E (DR-CVS-022) incorporated this change. Also, a new deburring fixture was made to obtain more equal deburring on both ends of each weld shield and to increase the overall length of the weld shields. Deviation request DR-CVS-023 was written to document the as-built deburring fixture, T2D800746A001, in Rev. B and to revise GPHS-XF-3620 to Rev. F accordingly. These changes were made and shown to reduce the incidence of initiation and/or propagation of cracks in the weld shield butt welds.

On May 9, 2000 C. E. Grosso and M. O. Smith of Westinghouse Government Services Group reviewed the status at the Oak Ridge National Laboratory of incorporating the integral weld shield manufacturing process into the CVS Manufacturing effort. They were pleased with the status, however, they recommended that 5 FQ weld shield cups should be completed for their review prior to full-scale weld shield fabrication for the FQ LANL return units. Weld shields have been blanked and are awaiting cleaning prior to butt welding.

2.5.2 Vent Notch Widening of LANL Returns

Deviation requests DR-CVS-014 and -016 were approved. DR-CVS-014 changed the primary certification inspection technique for the cup radius from optical comparator to the coordinate measuring machine and designated the toolmaker's microscope in the comparator mode as the back-up technique/equipment. DR-CVS-016 clarified the reporting of dimensions for cup certification inspection.

The nine EU shield cups returned from LANL have been fully processed. The averages and standard deviations for the widened vent notch dimensions are as follows: 0.530 ± 0.022 mm wide and 0.172 ± 0.006 mm deep. All of the notch dimensions were within the specified limits of 0.45/0.60 mm wide and 0.15/0.20 mm deep. Nonconformance report NCR-CVS-017 was submitted to and accepted by the ORNL Material Review Board because of other out-of-tolerance dimensions as well as pre-existing dye penetrant indications. These shield cups will remain as EU units and are awaiting certification review. Once the review is complete (and the necessary external NCR approval is received) they will be ready for vent cup assembly work, i.e. welding the 3 integral weld shield (IWS) tabs into place. After the shield cups are certified they will be processed as shield cup assemblies, packed, shipped, and recombined with their vent cup assemblies at LANL per the new Special Instruction Deviation Request SIDR-CVS-003.

Dimensional inspection of the 59 Flight Quality (FQ) shield cups returned from LANL has been completed per SIDR-CVS-003. The radius of cup 3625-26-3000 was found to be below the required minimum just as it was when it was sent from Y-12 to LANL originally. This feature was accepted for FQ use after review by the necessary Material Review Boards in 1993 (Nonconformance Report NY4383OR93), thus it is still FQ. The other 58 FQ cups meet all dimensional requirements. Eight FQ cups have been given their final acid clean. They are ready for certification review and subsequent weld shield tab-to-cup welding. The remaining 51 FQ cups are awaiting their final acid clean. The CVS Cleaning Area and the Plating Shop in Building 2525 at ORNL were shutdown for housekeeping and safety concerns. The two areas, which are adjacent to each other, were addressed separately to facilitate a faster startup for the CVS Cleaning Area. After a shutdown of approximately 3 weeks to address the concerns and make improvements, the CVS Cleaning Area was given permission recently to resume operations.

3. BASE TECHNOLOGY PROGRAM AND TECHNICAL SUPPORT ACTIVITIES

3.1 TECHNICAL SUPPORT FOR ARPS AMTEC CELL DEVELOPMENT

3.1.1 Introduction

The AMTEC cell is one of the primary thermal to electric conversion technologies being considered for future NASA outer planetary space missions. These cells use refractory metal alloys as materials of construction and sodium (Na) as a working fluid. ORNL is providing technical support to the AMTEC development program by providing materials fabrication, mechanical property data support, and component joining fabrication with the electron beam (EB) welding process. Nb-1Zr has been the primary material for the cell components developed for the ARPS Program. Oxidation concerns with this alloy have lead to the study of Mo-41Re as an alternate material. Mo-Re alloy sheet is being produced for evaluation in AMTEC development cells. Oxidation studies are being conducted on materials for the AMTEC application.

3.1.2 Oxidation Studies

Oxidation experiments to determine the behavior of Mo-41Re in low pressure oxygen environments were continued. Tests in vacuum are conducted by first evacuating the system to a low base pressure ($\leq 10^{-6}$ Pa) and then opening a micrometering valve to admit either pure oxygen or argon containing a known concentration of oxygen until the desired pressure is achieved. Tests were also conducted in argon (~5 vppm oxygen) at 76,000 Pa (1 atm). After evacuating the system, the vacuum system valve was closed and the test system pressurized to 1 atm. Excess pressure was relieved through an oil bubblier.

Weight Change

Results from exposures to pure oxygen at reduced pressures are shown in Fig. 1. At 10^{-3} - 10^{-4} Pa (10^{-5} - 10^{-6} torr) small weight gains were observed that generally increased with temperature. However, at 10^{-2} Pa (10^{-4} torr) weight losses were measured that became significantly larger at 800-900°C. In Fig. 2, the weight change rate is shown as a function of partial pressure of oxygen (P_{O_2}).

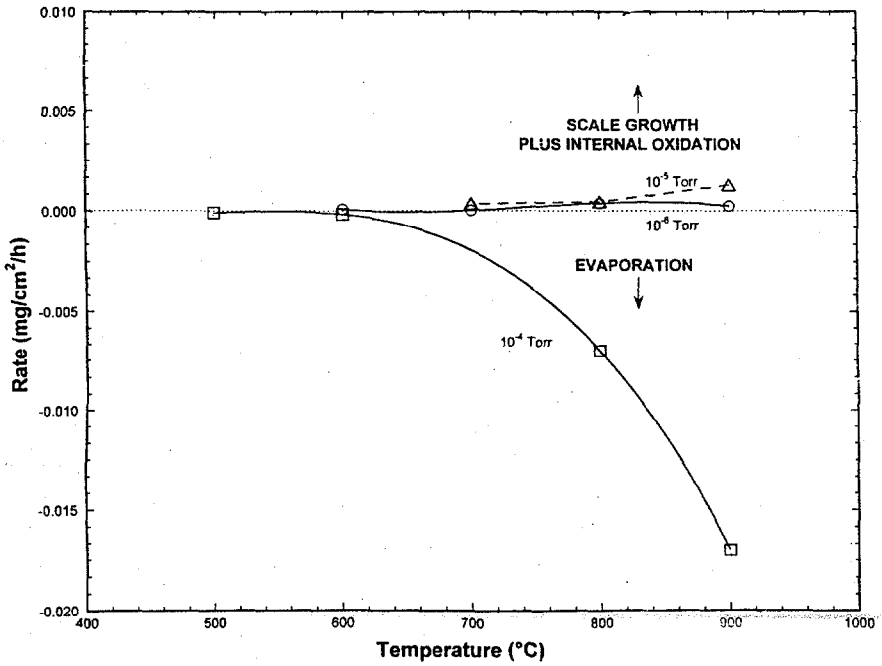

Fig. 1. Oxidation of Mo-41 Re for 500 h in low P_{O_2} vacuum.

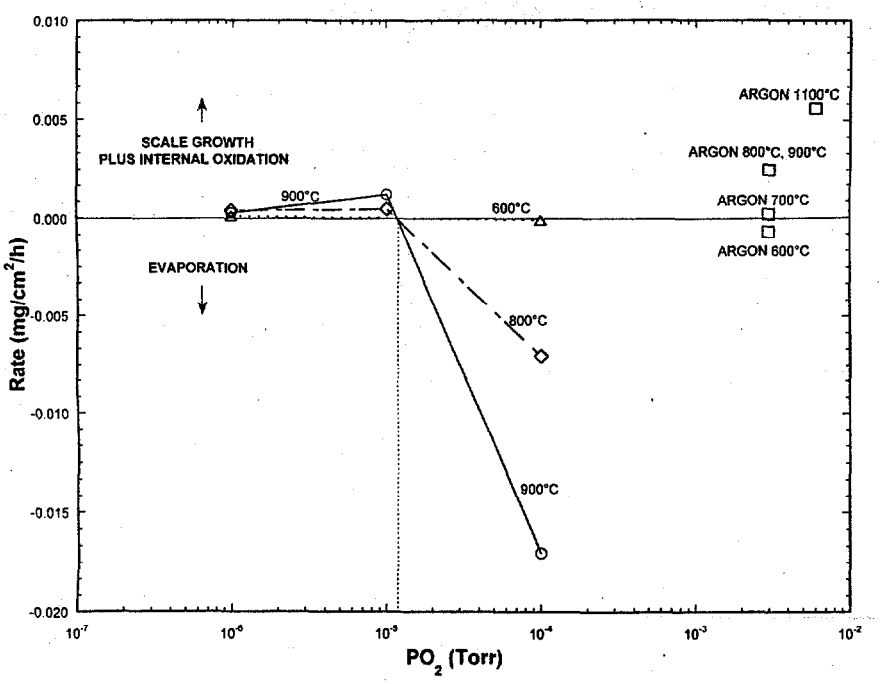

Fig. 2. Oxidation of Mo-41% Re for 500 h in low P_{O_2} vacuum and argon.

Results in argon (1 atm) are shown in Fig. 2 and Fig. 3. In contrast with the results in vacuum, weight gains were measured at the higher temperatures and only at 600°C was a weight loss measured.

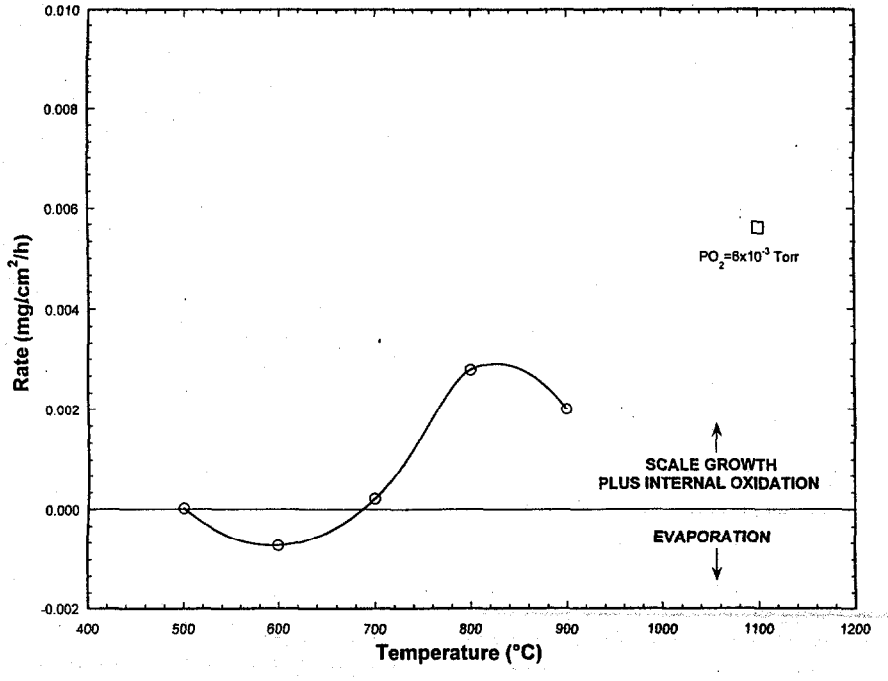

Fig. 3. Oxidation of Mo-41% Re for 500 h in argon (1 atm) with $P_{O_2} = 3 \times 10^{-3}$ torr.

Microstructural Changes

The surface and grain structure of Mo-41Re after annealing for 4 h at 1400°C followed by exposure to argon (5 O_2-15 N_2) for 100 h at 900°C is shown in Fig. 4. Under these conditions the sample picked-up ~300 wppm oxygen and there was little change observed microstructurally. However, after longer times a duplex reaction zone developed as shown in Fig. 5. X-ray and microprobe analyses identified the outer layer at MoO_2, but the reaction zone beneath the MoO_2 was fine-structured and difficult to analyze precisely. Microprobe analysis of a sample exposed at 1100°C indicated several different compositions of Mo, Re, and O. It is likely that this region contains MoO_2 since it was very hard (~1375 DPH) together with Mo-Re alloy. In one analysis, the Re content was above that in the base alloy, an indication that some depletion of Mo occurred due to formation of MoO_2. But the analyses are certainly dependent on which phases and how much of each are included in the microprobe spot size. In Fig. 6, a plot of weight change versus time is shown along with the depths of the outer and inner reaction zones. Note that the growth of the outer and inner reaction zones occur at approximately the same rates at 900°C.

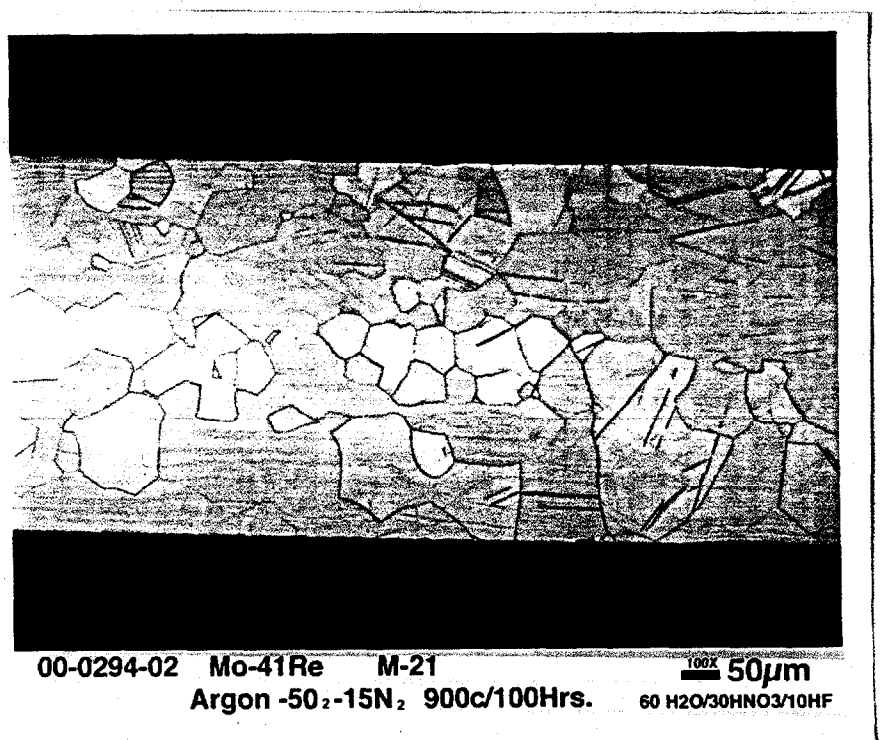

Fig. 4. Photomicrograph showing grain structure of Mo-41% Re after annealing for 2h at 1400°C and oxidation in argon.

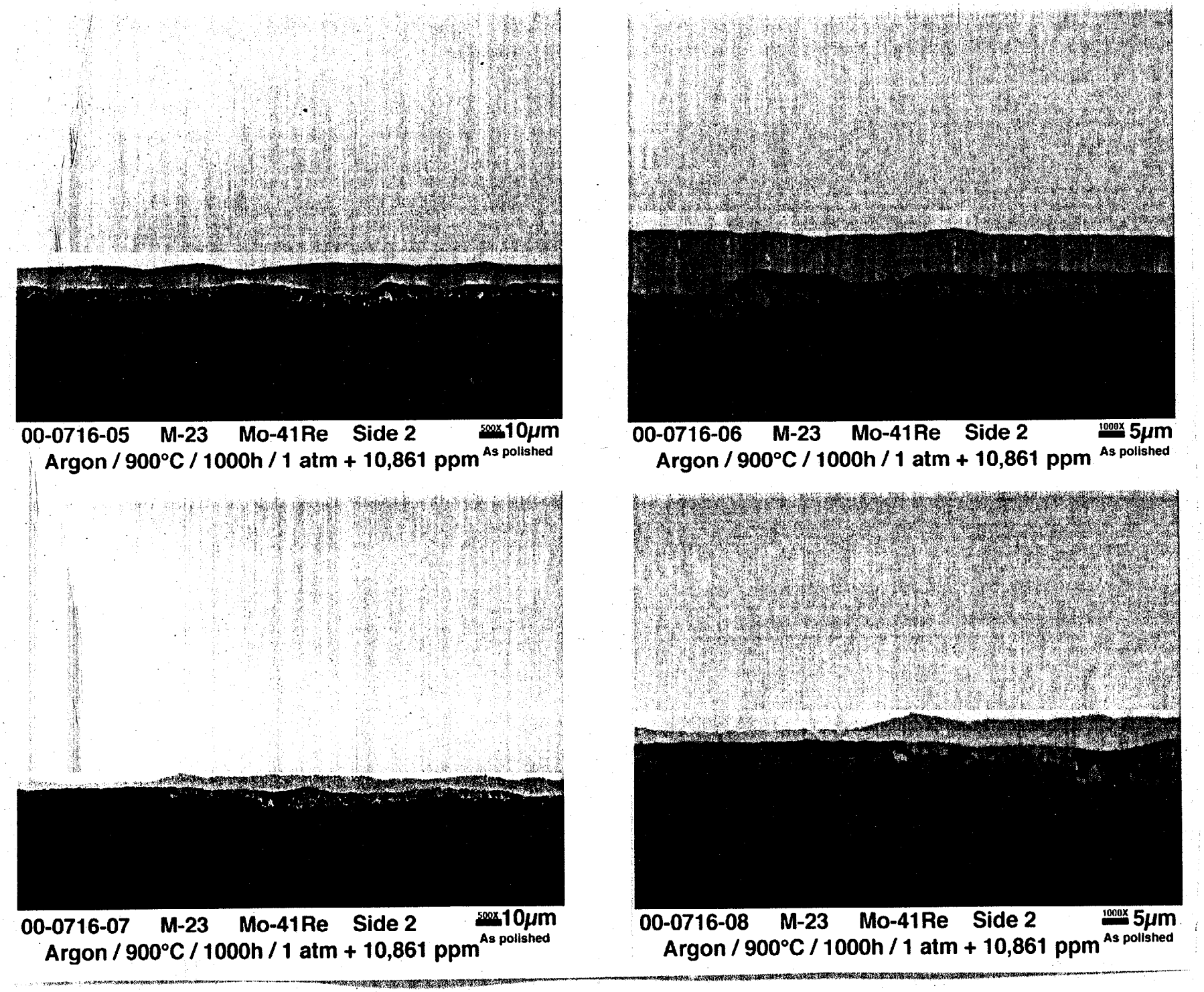

Fig. 5. Mo-41% Re with duplex reaction zone after oxidation in argon.

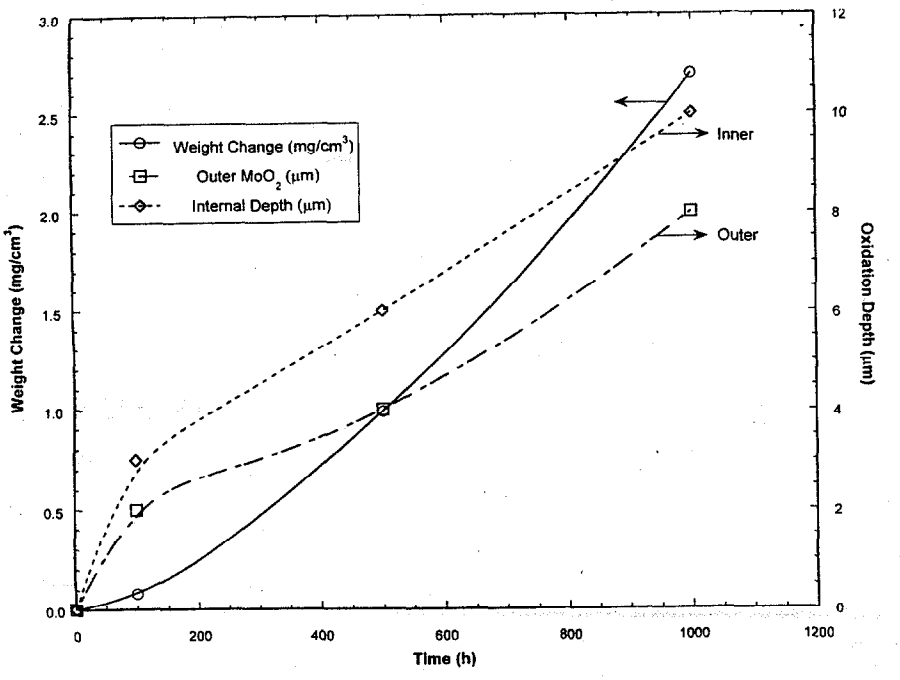

Fig. 6. Oxidation of Mo-41% Re at 900°C in argon (1 atm/3 x 10^{-3} torr P_{O_2}).

3.1.3 AMTEC Cell Fabrication Development

Fabrication of AMTEC cell components was performed for AMPS during this reporting period. Pump out ports on the condenser caps for future cells were electron beam welded and returned to AMPS. These were joined with the welding parameters for the pump out port design which is perpendicular to the cap. These subassemblies were used in test cells.

Drawings were reviewed and comments provided to AMPS on possible new welded feedthrough designs. These designs are intended to minimize the coarse-grained Nb-1Zr material that results from brazing feedthroughs in the condenser cap.

Welding fabrication of AMTEC cell components for the EPX -01-E5 was initiated. The BASE tube assemblies were welded to the BASE support plate without any evidence of insulator cracking. Difficulties were encountered with joint fit up during assembly by the AMPS personnel. A feedthrough insulator was broken while assembling cell walls. It was concluded that cell components now most likely have joints with interference fit since the enchant cleaning time has been reduced and less material is removed from the surfaces. Machining dimensions must be modified to accommodate etching procedure changes. The assembly of the cell continued until the artery was broken. The cause of the breakage was not certain. Some components from this cell will be salvaged and used for another cell assembly next quarter.

A test electron beam weld was made on a BASE support plate to an evaporator for determination of weld penetration in this Mo to Nb-1Zr joint. A previous weld had exhibited excessive penetration for the current joint design. The test weldment was sectioned and examined in metallography. The weld had no cracks or defects present in the four cross sections examined. The measured weld penetration was nominally 1.3 mm which is less than the desired 1.55 mm. An additional weld will be required to optimize this weld.

3.1.4 Molybdenum-41% Rhenium Alloy Sheet and Foil Production

Machining of components from Mo-41% Re alloy plate to produce one AMTEC mock-up cell was continued during this reporting period. A mid-cell wall rib, one condenser cap, and a hot-end BASE support plate were successfully completed. Figure 7 is a photograph of the Mo-41% Re hot-end BASE support plate. Although the material is difficult to machine, the cell components produced to date have dimensions that meet the drawing tolerances. This completes the machining of cell components planned to demonstrate the fabricability of Mo-41% Re alloy.

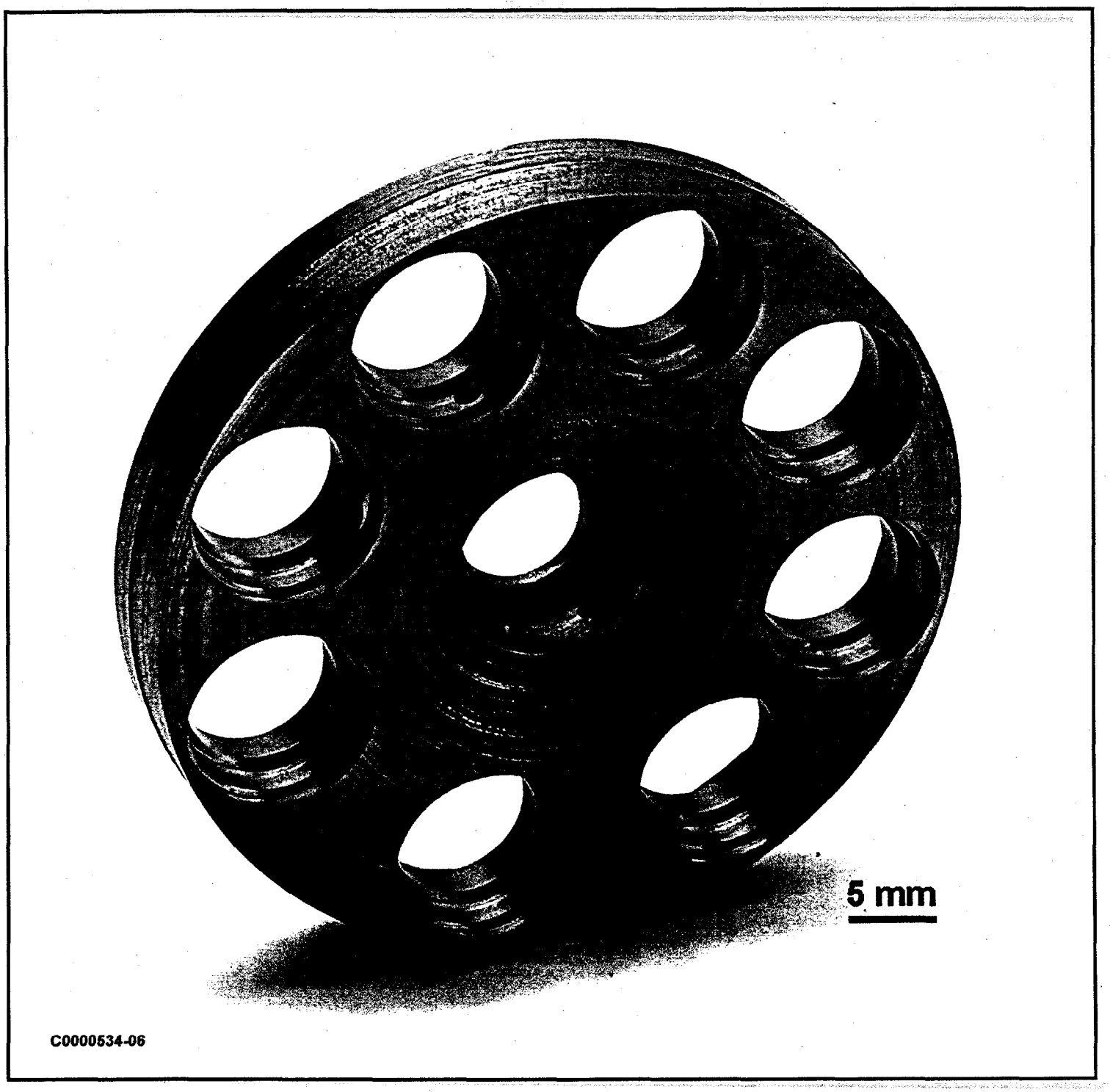

Fig. 7. Photo of Mo-41% Re hot-end BASE support plate.

Welding development tests were performed on 0.5 mm thick sheet of Mo-41% Re. Welding parameters are being established for seam welding this sheet into AMTEC cell walls. As found in previous welding evaluations, the weldability of the alloy has been excellent. Cell walls without reinforcing ribs will also be fabricated.

In response to a request from AMPS to supply some Mo-41% Re transition rings and flanged rings for a new artery/evaporator assembly being developed, material was processed and parts fabricated to their drawings. One of the component thicknesses required rolling the material to approximately 6 mm. Material was already available for the other ring component. Machining was completed for five Mo-41% Re rings (0.325 inches OD x 0.187 inches ID) and four flanged rings. These were supplied to AMPS for use in the evaporator welding fabrication.

A calibration run for heating of Mo-41% Re billets prior to extrusion was performed using the MR3 ingot in a thin-wall (1.5 mm) molybdenum can. The calibration showed that the billet temperature was about 150°C above the can temperature, as measured with a two color optical pyrometer, and also that the initial cooling rate of the billet after heating is about 150°C per minute. This information was used for extrusion of the MR3 billet. Processing of 11 kg of powder was begun for a new Mo-41% Re alloy billet identified as MR4. Electron beam melting of the powder was started. Additional carbon master alloy was produced for melting this material. Carbon analysis shows about 80% retention of carbon following electron beam melting.

3.2 ALLOY DEVELOPMENT AND CHARACTERIZATION

3.2.1 EFFECT OF GRAIN SIZE ON IMPACT DUCTILITY OF Ce+Th-DOPED DOP-40 IRIDIUM ALLOYS

DOP-40 iridium is being developed as a potential substitute for DOP-26 iridium in future deep-space missions. The original goal of our alloy development program was to replace all of the radioactive thorium in DOP-26 iridium with non-radioactive cerium. However, our studies showed that, although Ce was effective in refining the grain size of Ir, it was not as effective as Th in enhancing grain-boundary cohesion [1]. Since grain size and grain-boundary cohesion both influence high-temperature impact ductility [2], our alloy design strategy now seeks to replace only part of the Th with Ce, with the former serving mainly as a grain-boundary strengthener and the latter as the grain refiner.

Having concluded that both Ce and Th were necessary, we decided to investigate how the metallurgical properties of DOP-40 iridium change with small changes in the thorium and cerium concentrations. The Ce and Th concentrations that were chosen fell within their allowable ranges in the current DOP-26 specification: 60±30 wppm for Th and <50 wppm for Ce. In the first part of this investigation, we investigated the effects of test temperature on the high-temperature impact ductility of DOP-26 iridium as a function of changes in the Ce and Th concentration [3]. In a more recent study we investigated the effects of annealing temperature (1300-1800°C) on the impact ductility of the same alloys impact tested at 1000°C [4]. In this study we investigate the effects of grain size on impact ductility.

The specimens used in this study were the same specimens that were previously used to determine the effect of test temperature and annealing temperature on impact ductility [3,4]. The seven DOP-40 heats were arc melted, drop cast, and rolled using the so-called old process. Their nominal Ce/Th dopant concentrations are listed in Table 1. Note that Al, which is added at a level of 50 ppm in DOP-26 iridium, was not added to any of the DOP-40 alloys. After hot rolling, the sheets were electrolytically cleaned in potassium cyanide and acid cleaned in a solution containing 3 parts HCl, 1 part HF and 1 part water. Tensile impact specimens were prepared as described elsewhere [5] and heat treated in vacuum for 1 h at temperatures of 1300-1800°C. Tensile impact testing was performed at temperatures from 800 to 1300°C on specimens annealed for 1 h at 1500°C and at 1000°C as a function of annealing temperature, all at a bullet velocity of 61 m/s. The fracture modes were determined using scanning electron microscopy. After impact testing, the undeformed ends were cut from the shoulders of each tensile specimen. Optical metallography techniques of polishing, etching, and measuring grain sizes (as described in ref. 5) were used to determine the grain growth as a function of annealing temperature. Grain sizes were measured by the method of linear intercepts in the short transverse (ST) direction with respect to the rolling direction. The confidence limits of the data are indicated by the number of intercepts (recorded in parentheses in the Table 2) counted for each data point.

Table 1. Nominal dopant levels of DOP-40 (Ir-0.3%W) alloys.

Alloy No.	Ce (wppm)	Th (wppm)
I-101	20	30
I-102	20	40
I-103	30	30
I-104	30	40
I-105	30	50
I-106	40	40
I-107	40	50

Table 2. Grain size of DOP-40 alloys at different annealing temperatures

Alloy	Annealing Temperature (°C)					
	1300	1400	1500	1600	1700	1800
I-101						
grain size (μm)	15 (1234)	18 (969)	21 (915)	36 (1296)	66 (773)	126 (431)
$(gs)^{-1/2}$	0.255	0.239	0.220	0.166	0.123	0.089
I-102						
grain size (μm)	17 (1140)	20 (1331)	22 (848)	40 (1290)	72 (740)	97 (545)
$(gs)^{-1/2}$	0.242	0.225	0.211	0.159	0.118	0.102
I-103						
grain size (μm)	17 (1134)	17 (1440)	22 (882)	41 (1240)	78 (700)	132 (409)
$(gs)^{-1/2}$	0.243	0.242	0.214	0.156	0.113	0.087
I-104						
grain size (μm)	16 (1187)	19 (890)	22 (869)	40 (1267)	70 (755)	102 (527)
$(gs)^{-1/2}$	0.246	0.229	0.211	0.157	0.120	0.099
I-105						
grain size (μm)	16 (1199)	21 (1299)	23 (815)	43 (1190)	81 (645)	117 (449)
$(gs)^{-1/2}$	0.249	0.219	0.207	0.153	0.111	0.092
I-106						
grain size (μm)	18 (1069)	22 (1543)	22 (809)	42 (1177)	75 (708)	144 (430)
$(gs)^{-1/2}$	0.235	0.216	0.211	0.154	0.115	0.083
I-107						
grain size (μm)	17 (1123)	20 (1335)	23 (823)	38 (1299)	70 (745)	101 (519)
$(gs)^{-1/2}$	0.240	0.222	0.210	0.161	0.119	0.100

Figure 1 (modified from Fig. 1 of Ref. 3) shows the temperature dependence of the impact ductilities of the seven DOP-40 alloys (heat treated 1 h at 1500°C) investigated in this study. Included for comparison are data for new-process DOP-26 annealed for 1 h at two different temperatures (1400 and 1600°C), taken from an earlier study [5]. The curve for DOP-26 annealed for 1 h at 1500°C is expected to fall between the curves for DOP-26 annealed for 1 h at 1400 and 1600°C. By comparing the curves for the various DOP-40 alloys annealed for 1 h at 1500°C with the expected curve for DOP-26 annealed for 1 h at 1500°C, it is concluded that the DOP-40 alloys are as good or better than the currently used DOP-26 alloy. The fracture modes of the DOP-40 alloys are similar to that of the DOP-26 alloy. At impact test temperatures of <1000°C, the alloys are all relatively brittle and fracture predominantly intergranularly (see Fig. 2a). At elevated temperatures (above about 1100°C) the alloys are ductile and fracture transgranularly with considerable necking (see Fig. 2c). At intermediate temperatures, the alloys undergo a brittle-to-ductile transition and fracture by a mixed intergranular/transgranular cleavage mode (Fig. 2b).

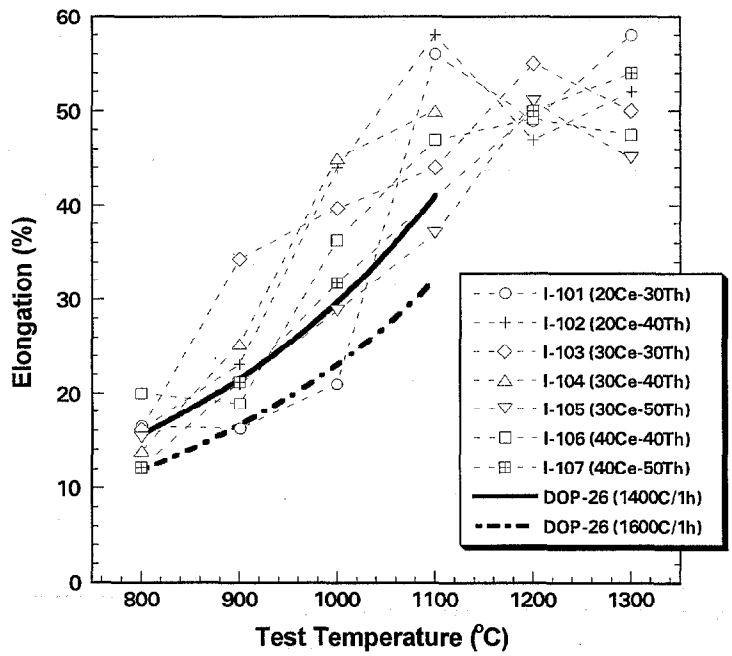

Fig. 1. Comparison of the temperature dependence of the impact ductilities of DOP-40 (annealed 1h at 1500°C) and DOP-26 iridium alloys annealed 1 h at 1400 and 1600°C. All tests carried out at a bullet velocity of 61 m/s.

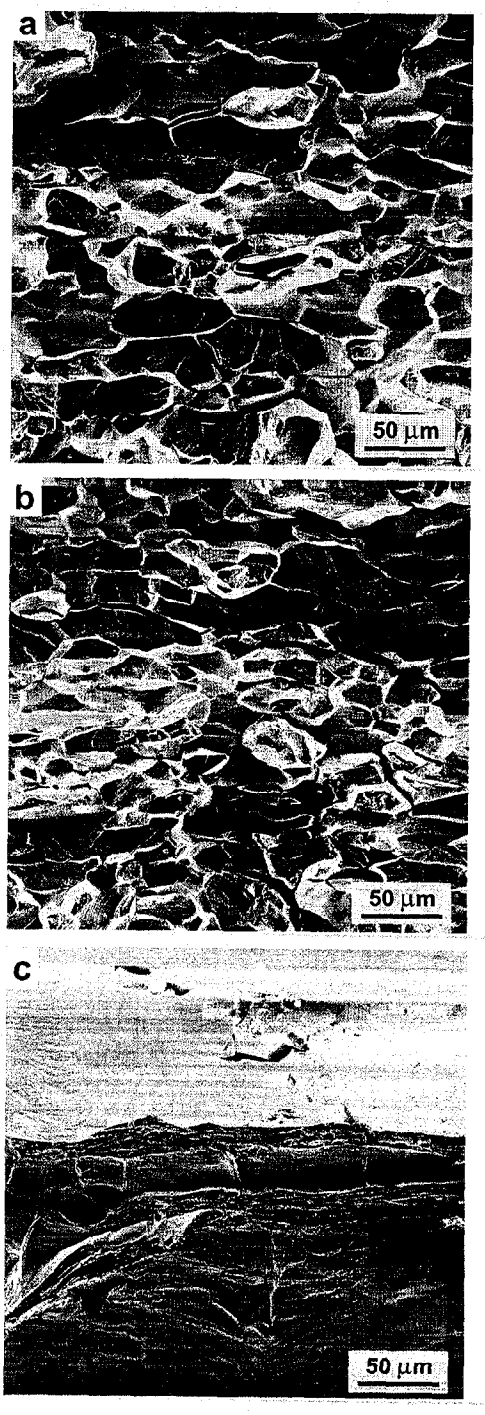

Fig. 2. Scanning electron micrographs showing typical fracture modes of DOP-40 alloys heat treated for 1 h at 1500°C and then impact tested at (a) 800, (b) 1000, and © 1300°C.

Figure 3 shows the effect of annealing temperature on the impact ductility of DOP-40 at 1000°C. The sharp drop in ductility is the result of increasing grain size with increasing annealing temperature. This can be seen in Table 2 and Figure 4 which shows the grain size of the impact specimens as a function of annealing temperature. In each of these figures, data for new-process DOP-26 (containing no Ce addition) are included for comparison [1,5]. These figures indicate that, with increasing annealing temperature, the grain sizes of the DOP-40 alloys increase while ductilities decrease. This result is consistent with the commonly observed deleterious effect of grain coarsening on the impact ductility of DOP-26 iridium [1,5]. The DOP-40 and DOP-26 data are comparable in this respect.

Using a model of stress concentrations induced by dislocation pileups at grain boundaries [1], it can be shown that, by plotting the impact ductility as a function of the reciprocal of the square root of grain size, the resulting straight line will give an indication of the grain boundary cohesive strength. The effectiveness with which different dopants affect the grain boundary cohesion can then be inferred by comparing the slopes obtained for different alloys. The data from this study are plotted in this manner in Figure 5. The solid line represents a straight-line fit of the data from all seven DOP-40 alloys. For comparison purposes the straight-line fit for data determined previously for old-process DOP-26 (containing no Ce) [1,5] are included in Fig. 5. The slope of the DOP-40 and DOP-26 lines are similar, suggesting that the grain-boundary cohesive strength of DOP-40 is similar to that of DOP-26. The data show that the ratios of Ce/Th used in this study do not significantly affect the grain boundary cohesive strength. This is consistent with the results of Gubbi, et al. on DOP-26 iridium alloys doped with 10-50 ppm Th and 30-50 ppm Ce [1].

In Fig. 1, it was shown that the tensile impact ductilities of the seven DOP-40 alloys (heat treated for 1 h at 1500°C) were comparable to or better than those of DOP-26 iridium given the same heat treatment. From a practical standpoint, it is the ductility after a given heat treatment that is most relevant (e.g., impact performance after accidental re-entry into earth atmosphere). In this respect, the DOP-40 alloys are as good as or better than the DOP-26 alloys. From a scientific perspective, however, it is important to compare the DOP-40 and DOP-26 alloys at similar grain sizes. This is done in Fig. 6 where the seven DOP-40 alloys having a grain size of 22±1 μm are represented by a single curve with error bars and are compared to the ductilities of DOP-26 having grain sizes of 22 and 27 μm. The data show that the impact ductility of DOP-40 with a grain size of 22 μm is comparable to that of DOP-26 with approximately the same grain size.

In summary, the grain sizes of Ce/Th-doped DOP-40 alloys (designated as ingots I-101 through I-107) were determined as a function of annealing temperature and were correlated with the impact ductilities. The grain sizes of the DOP-40 alloys were observed to increase with increasing temperature while ductilities decreased. This result is consistent with the commonly observed deleterious effect of grain coarsening on the impact ductility of DOP-26 iridium. Using a model of stress concentrations induced by dislocation pileups at grain boundaries, it was shown that the ratios of Ce/Th used in this study do not significantly affect the grain boundary cohesive strength. Additionally it was shown that the impact ductility of DOP-40 with a grain size of 22 μm is comparable to that of DOP-26 with approximately the same grain size. However, the ductility of DOP-40 after 1-h anneal at 1500°C was better than (or at least as good as) that of DOP-26 given the same heat treatment. The reason for this is that the DOP-40 alloys exhibit slower grain growth than DOP-26 at temperatures below ~1600°C.

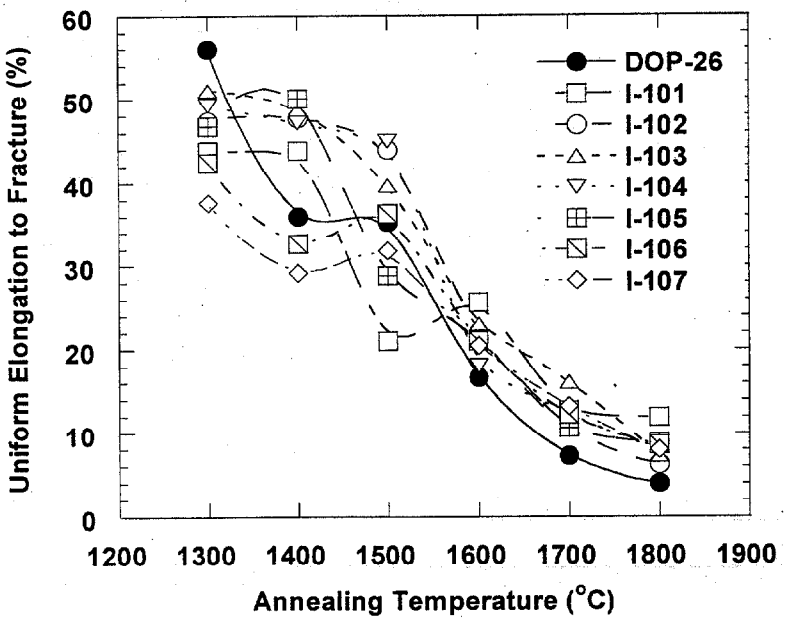

Fig. 3. Effect of annealing temperature on the impact ductilities of DOP-40 iridium alloys at 1000°C (bullet velocity, 61 m/s). Data for new-process DOP-26 impact tested at 980°C (from ref. 1) are included for comparison.

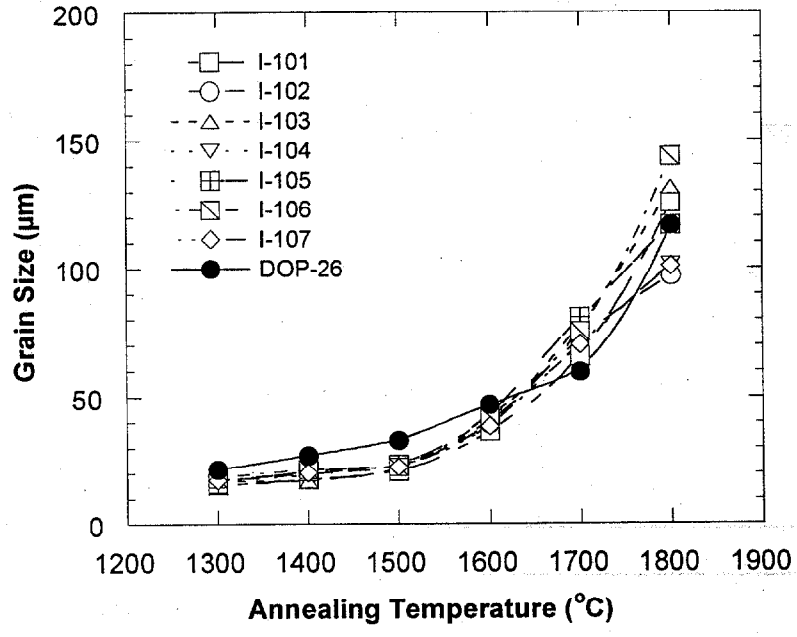

Fig. 4. Effect of annealing temperature on the grain growth of DOP-40 iridium alloys. Data for new-process DOP-26 (from refs. 1,5) are included for comparison.

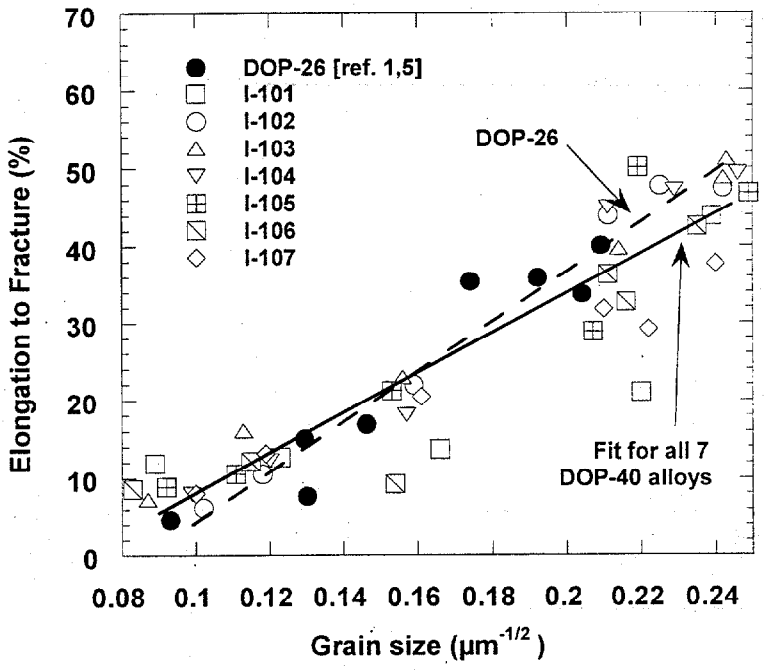

Fig. 5. Variation of impact ductility with the inverse square root of grain size for DOP-40 iridium alloys. Data for new-process DOP-26 (from ref. 1,5) are included for comparison.

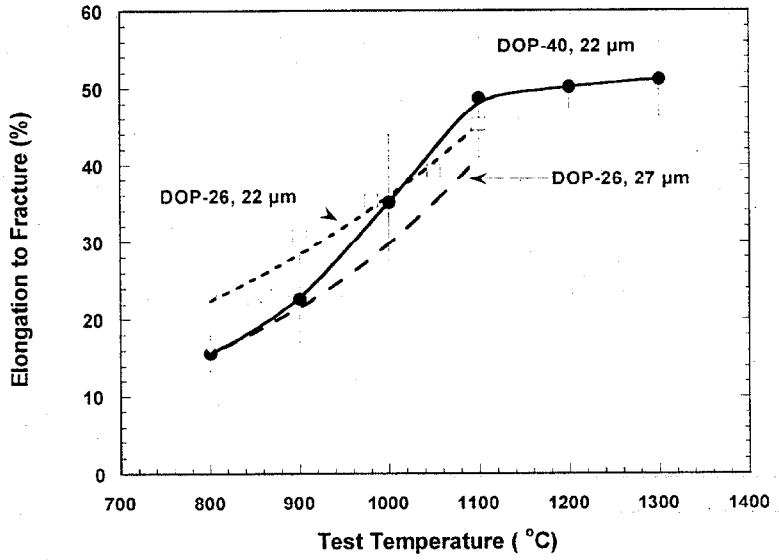

Fig. 6. Comparison of the temperature dependence of the impact ductilities of DOP-40 and DOP-26 (new process, ref. 5) iridium alloys.

References

1. A. N. Gubbi, E. P. George, E. K. Ohriner, and R. H. Zee, Metall. Trans. 28A (1997) 2049.

2. C. T. Liu, H. Inouye, and A. C. Schaffhauser, Metall. Trans. 12A (1981) 993.

3. E. P. George, E. K. Ohriner, and E. H. Lee, "Sensitivity of the High-Temperature Impact Ductility of DOP-40 Iridium to Small Changes in Ce and Th Concentration," attachment to letter, J. P. Moore to W. J. Barnett (1998).

4. E. P. George, E. H. Lee, C. G. McKamey, and E. K. Ohriner "Effect of Annealing Temperature and Changes in Ce and Th Levels on Impact Ductility of DOP-40 Iridium at 1000°C," Attachment to letter, J. P. Moore to W. J. Barnett, Sept. 30, 1999.

5. C. G. McKamey, A. N. Gubbi, Y. Lin, J. W. Cohron, E. H. Lee, and E. P. George, ORNL-6935, Oak Ridge National Laboratory, April 1998.

3.3 TECHNICAL SUPPORT FOR ADVANCED LONG TERM BATTERY

3.3.1 Background

The fuel in the advanced long term battery will be contained within nested capsules fabricated from Haynes Alloy No. 25. This material is a solid solution cobalt base alloy with excellent fabricability, corrosion resistance, and mechanical strength. Although the alloy was used several decades ago for fuel encapsulation, re-evaluation and qualification of a newly-produced heat was judged to be an essential part of the safety test plan for the battery (ref. 1). A large heat of Haynes 25 was procured for all testing and evaluation. The Oak Ridge National Laboratory (ORNL) was given the responsibility for producing the mechanical properties needed for the evaluating the lifetime of welded capsules under envisioned conditions of temperature, pressure, and age. The test plan identified uniaxially-stressed tensile, creep-rupture, and low-stress creep tests on base metal and weldments. As-received and aged materials were included in the testing plan. About 60 tests on base metal and 60 tests on weldments were specified. Pressurized capsule tests were identified in the plan. To meet the testing performance standards required for a safety analysis, testing equipment assigned to the program had to be updated and the standard operating guidelines had to be revised and critically reviewed.

3.3.2 Material and Specimens

The long-time aging of base metal sheet specimens reached 10,000 hours of a planned 12,000 hours.

Ten welded plates of Haynes 25 were received from Babcock and Wilcox of Ohio, Inc. (Mound Plant). Distortion, normally associated with welding this configuration, produced a kink amounting to a few degrees across the weld line. We are concerned that a kink in machined specimens might adversely affect the mechanical properties of the weldment specimens. An option was to straighten the specimens by bending prior to aging and testing, but the effect of the cold work was of concern. Some exploratory testing was performed. A machined sample was straightened in a three-point bend rig. An as-machined weldment specimen, a flattened weldment specimen, and a base metal specimen were embrittled by aging for 92 hours at 850°C, then tensile-tested at room temperature. All aged specimens showed about the same embrittlement, as shown in Table 1, and failures occurred in the base metal away from the weld. The flattened condition was judged to be best for the weldments specimens. Flattened test specimens were ordered.

Table 1. Results of Tensile Tests to Examine the Influence of Flattening on Weldment Specimens

Specimen Number	Condition	Ultimate Strength (ksi)	Elongation (%)	Failure Location
HS 02-01	Base	145	56.6	base
HS 03-30	Base + age[a]	153	26.0	base
HS25W03	Weld + age[a]	128.9	21.1	base
HS25W01	Weld + flatten + age[a]	134.0	25.2	base

a. 92 hours at 850°C

3.3.3 Creep and Creep-Rupture Testing

Six of the fourteen creep and creep-rupture machines were operated. One creep-rupture specimen (CR-BM 05) ruptured after 3716 hours. A new creep rupture test (CR-BM-02) was started at 700°C and 24 ksi. The creep testing status is provided in Table 1.

Table 2. Summary of Creep Tests

Test ID	Temperature (°C)	Stress (ksi)	Time (hours)	Creep Rate (%/hour)	Creep Stage
CR-BM-01	650	30	2500	.00023	primary
CR-BM-02	700	24	100	.0017	primary
CR-BM-03	750	18.5	3500	.00051	secondary
CR-BM-04	800	14.4	3500	.00075	secondary
CR-BM-05	800	15	3716	.0011	ruptured
CR-BM-06	850	9	3400	.00051	primary

3.3.4 Pressured-Capsule Testing

Two capsules were assembled into canisters and installed at testing stations. Vacuum pumping capability was installed and the data acquisition systems were activated to collect pressure data and temperatures at six locations. Temperature checkout studies were undertaken to locate the optimum positions within the furnaces for the canisters in order to minimize temperature gradient in the test capsule. The minimum temperature gradient achieved was 5°C. Further changes in the furnace insulation were planned.

3.3.5 Reference

1. M. F. McKittrick and S. T. Christenbury, *Preliminary Safety Test Plan for the Advanced Long Term Battery (ALTB) Heat Source (HS)*, Teledyne Brown Engineering – Energy Systems, Hunt Valley, MD, April 30, 1999.

3.4 B-SCAN AND ULTRASONICS

3.4.1 Background

In support of the Cassini mission to Saturn, ORNL and the Y-12 Plant were involved in the production of clad vent sets for use in radioisotope thermoelectric generators (RTG). As part of this effort, Y-12 developed a new ultrasonic inspection for the closure weld, based upon previous efforts used in the Galileo and Ulysses programs, but including new equipment and a new B-scan technique to identify benign problems such as weld shield fusion and weld mismatch. The basic inspection was documented by M. W. Moyer in "Ultrasonic Inspection of General Purpose Heat Source Clad Vent Set Closure Welds," a report (Y/DW-1310) dated May 17, 1994. However, the B-scan technique was developed later but not fully documented. This effort is to produce a comprehensive report to document the full ultrasonic effort and show typical results from actual CVS welds.

3.4.2 Development of B-Scan Inspection

The basic Top Scan ultrasonic inspection using amplitude and time-of-flight data was usually sufficient to certify the weld quality of fueled clads produced for the Cassini Mission. A threshold was set for a "number 8" flaw which was determined to be equivalent to a 0.132 mm (0.0052 in.) slot in the standard. If a fueled clad had no indications that were above the threshold, the weld was judged to be sound. Only when signals were detected above the threshold was it necessary to acquire additional data.

For the B-scan inspection, the index axis of the scan was adjusted for the maximum signal and a single RF waveform scan consisting of 360 waveforms was taken as the fueled clad was rotated about its axis. The bipolar RF waveform data was rectified to produce a unipolar video waveform before data acquisition. Waveform data were acquired from both sides of the fueled clad, i.e. with the fueled clad oriented in both the Vent Up and the Vent Down positions. Waveform data were taken only from fueled clads with indications above the threshold because the data sets were roughly 10 times the size of the amplitude/time-of-flight data sets. An example B-scan is shown in Figure 1. The vertical axis is the scan axis, which is the angular location of the fueled clad. The horizontal axis is the time of the waveform. Two example waveforms are shown which represent the data at 127 and 305 degrees. The schematic shows that the signal enters the fueled clad at the top surface and is reflected from the weld in areas where there are defect or geometric conditions. The waveform amplitude is displayed as color that is calibrated in engineering units.

B-scan data as well as amplitude and time-of-flight data were received from LANL for 29 welded fuel clads. All of the fueled clads had at least one area where the ultrasonic signal was large enough to cause the fueled clad to be classified as nonconforming.

During this initial phase of inspection it became evident that there were several benign conditions such as weld shield fusion (WSF) and wall thickness mismatch that might be generating the signals which caused the fueled clads to be nonconforming. The weld penetrating through the fueled clad wall into the weld shield causes weld shield fusion. When this condition occurs, there is a change in the weld root geometry that can cause an ultrasonic signal to be reflected from the portion of the weld root that tacks into the weld shield. The distance of the gap between the fueled clad wall and the weld shield will determine the amplitude of the reflection. Thus, if the weld shield is touching the fueled clad wall, the reflection will be small, while if there is a gap between the weld shield and the fueled clad so that the weld protrudes across the gap to tack into the weld shield there will be a larger reflection. Add mismatch to this condition and you can have a complicated signal return. In addition, the propagation of Lamb waves is affected because the effective wall thickness of the fueled clad has changed. This is a benign condition even though signals greater than the reject level may be detected.

The standard ultrasonic inspection consists of sending a Lamb wave down the wall of the fueled clad and detecting the reflection from any interfaces in the weld. The amplitude of the signal is recorded. Signals from known size artifacts (electro-discharged machined slots) in a standard are used to calibrate the system. A time-of-flight measurement was implemented to try to detect the position of the reflecting surface that caused the signal. Since WSF should have some width, the signals from the WSF should occur away from the weld centerline.

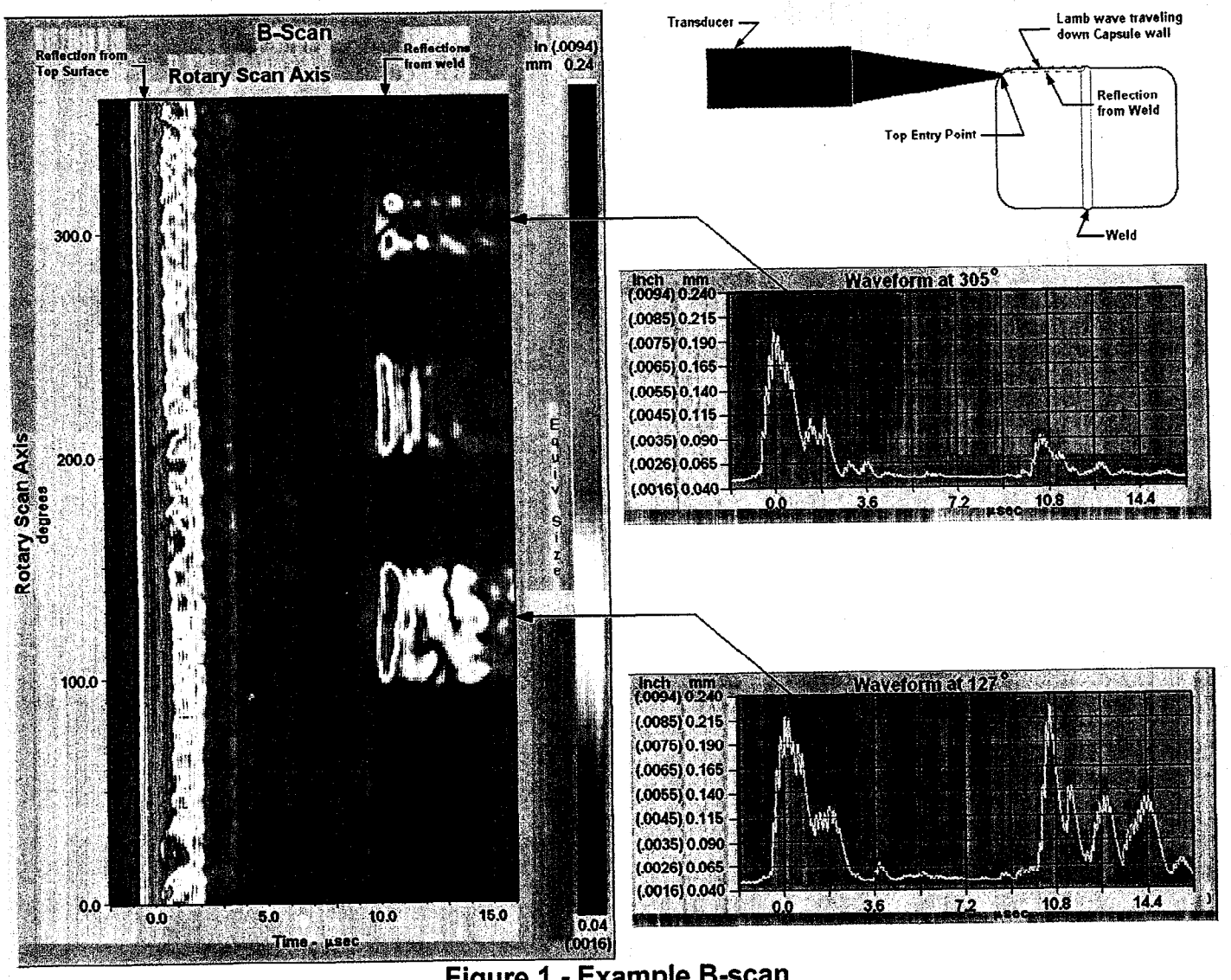

Figure 1 - Example B-scan

Since the Lamb wave inspection generates several different modes of Lamb waves, each with a different velocity, several signals will be detected from a well-defined reflector. The time of the signal will depend upon the Lamb wave velocity. For a reflection from a reference slot such as the electro-discharged machined slots in the standard, the first signal received (from the highest velocity Lamb wave) is the largest. It has been observed on data received from LANL on several of the GPHS fueled clads that sometimes, one of the slower Lamb waves produces the largest signal. This can cause the signal to appear to have been reflected from a point that is further from the transducer.

In order to try to identify the types of signals obtained from the different defects, we evaluated the B-scan data from the 29 fueled fueled clads that had signals above the reject level.

We identified several signal types. The first category includes short signals located near the weld centerline in the weld overlap area between 10 and 30 degrees. Cracking in the weld tie-in area during production of the Galileo/Ulysses GPHS fueled clads led to the initial development of the first-generation ultrasonic test for girth weld inspection at the Savannah River Plant. It was found that this cracking was caused by the low melting Ir_5Th eutectic at the weld centerline. In the area of the overlap where the second weld pass is less than fully penetrated (as the weld current is reduced at the end of the weld), grain boundary separation occurs under the influence of thermal and mechanical stresses. This can produce weld cracking.

The second category of signals was obtained from an area of weld root suckback with or without an external weld bulge. This condition occurs in the weld overlap region because the weld seals the vent grooves and internal pressure within the fueled clad causes the weld to bulge with corresponding suckback at the back of the weld. The size of the signal and the time of the signal depends upon the sharpness of the corner at the edge of the weld.

The third category is porosity. A signal would be obtained only if the porosity occupied a significant percentage of the wall thickness. Generally, large pores would produce short sharp signals. Although porosity has been detected by tangential radiography in one fuel clad, it was too small to be detected with ultrasonics.

The next category consists of a rather long uniform signal. The data from most of the fueled clads (25 of 29) fall into this category. In general the first signal originates from near the weld centerline and is followed by several roughly parallel signals. The signals that follow the first signal are from different Lamb wave modes that have slower velocities. In some cases, the first signal is the largest from one side of the weld, while the second or third signal may be larger when inspected from the opposite side of the weld. When the second or third signal is larger, a false time-of-flight distance is measured since the system detects the largest signal in the gate. The long uniform signals are from a geometric reflector such as mismatch on the weld inside surface.

Other conditions could also show a long linear indication. A long section of WSF would cause a long linear indication. However, the fueled clad wall mismatch signal is distinctly different from WSF. It is extremely doubtful that a crack could cause this type of response because a crack would be rough; and if it extended the length of these indications, it would break through the fueled clad wall. It is also possible that a long linear signal could be caused by lack-of-penetration. With the automatic welding it is doubtful that the weld current could drop enough to cause a long section of lack-of-penetration. However, it is recommended that tangential radiography be used to identify the mismatch condition and confirm that the signal is not caused by lack-of-penetration. It might also be possible in future programs to use a normal ultrasonic inspection to identify the fueled clad wall mismatch.

Examples of B-scan results from these categories of defects are presented in the final report.

4.0 PLUTONIUM PRODUCTION STUDIES

4.1 TARGET DEVELOPMENT

4.1.1 Dosimeter Targets

The objective of the dosimeter target irradiations is to characterize 238Pu production, especially ^{236}Pu content, at various locations in each reactor. Dosimeter targets were designed, fabricated, and inserted into both the INEEL/ATR and the ORNL/HFIR. The resulting data will provide a firm basis for selection of appropriate ^{237}Np (n,2n)/^{236}Pu and ^{237}Np (γ,n)/ ^{236}Pu cross section data sets.

Six dosimeter capsules, which had been irradiated in the ATR, were shipped to ORNL for isotopic analysis to determine ^{236}Pu content.

The ATR dosimeter capsules had radiation doses larger than anticipated. Several modifications to the original post irradiation examinations were required in order to maintain low doses to workers. The early flowsheet was also based on cutting open the can and removing the irradiated NpO_2 wire. The flowsheet has been modified such that the can is dissolved into nitric acid, the NpO_2 wire is filtered from the resulting solution, and the NpO_2 wire is then dissolved using nitric acid with a small amount of hydrofluoric acid. Analysis results are expected in the fall of 2000.

4.1.2 Target Pellet Tests

A conceptual design for a test pellet was developed in conjunction with personnel at INEEL/ATR. A conceptual design was also developed for the ORNL/HFIR. The basic feature of the designs for target pellets is the use of an encapsulated mixture of Al and NpO_2 that has been compressed to 80–90% of theoretical density in the form of a small pellet. These pellets are enclosed in an aluminum liner to ease the handling process while targets are fabricated. Once several pellets have been fabricated, they can be inserted into a target capsule.

Safety analyses for the pellet targets were performed by ATR staff. The safety analysis confirmed that the targets will generate a significant heat load. Therefore, adequate heat transfer will be the key to ensure target survival (e.g., avoid melting). The gap between the pellets and the cladding was identified as having the most resistance to heat transfer. Maintaining a maximum radial gap of 0.001" was identified as a critical parameter of the target fabrication process.

A pellet pressing test program was developed to examine various characteristics of the final pressed pellets. Methods for pellet powder blending, pellet pressing, and pellet quality assurance were developed on cold mixtures of aluminum and cerium oxide. These methods were then applied to the NpO_2 pellet pressing.

Fifty NpO_2 pellets were fabricated in the glove boxes containing special pellet pressing equipment. NpO_2 was mixed with aluminum powder to fabricate pellets with 5, 10, and 20% by volume NpO_2 and pressed to 80% and 90% of theoretical density. The pellets were thermally cleaned for 2–3 hours at 350 °C and cooled under a vacuum. Each pellet was placed in an ionization chamber/electrometer to record base line readings that could be attributed to ^{233}Pa decay for future evaluations. The pellets were then radiographed and examined for defects and proper NpO_2 powder distribution. All pellets passed inspections and were loaded into six target tubes.

Each target tube contained eight pellets: two of the 5 vol.%-CeO_3 pellets pressed to 80% density; two of the 20 vol.%-CeO_3 pellets pressed to 90% density, four of the 10 vol.%-CeO_3 pellets pressed to 90% density, and a dosimeter package. The target tubes were then sealed by welding aluminum caps on the ends of the target tubes. The welded tubes were radiographed and helium leak checked. The target tubes were then hydraulically compressed to collapse the tube onto the target stack. The initial and final diameters of the targets were measured in order to verify that the target tube had been collapsed onto the pellet. Targets were also radiographed to check the gap between the target stack and the target tube. Each target underwent a final leak check using a helium leak detector and a dye penetrant weld/leak test.

A data sheet for each individual pellet was produced to record powder content, physical characteristics, and target tube assignments. Detailed document packages were created for the targets describing the physical characteristics, pellet stack, and dosimeter assignment. All material certifications, inspections, and examinations were presented in the target package. The data package was reviewed and accepted by both ORNL QA and INEEL/ATR QA. The targets were shipped to INEEL and are currently being irradiated.

4.1.3 Waste Disposition

This effort begins with data from the FY1999 studies and looks at technologies for waste minimization proposed in the early study. Of particular interest, is the desire to segregate waste in order to minimize TRU waste and allow treatment of selected waste streams. The solid waste is further subdivided into porous and nonporous waste. These waste streams will require different approaches to waste pretreatment and minimizing action.

We are currently investigating three methods of removing radioactive contamination from miscellaneous parts and equipment as a mechanism to eliminate a substantial portion of the non-porous radioactive waste. The three methods are (1) electrolytic decontamination, (2) chemical extraction with the TechXtract method, and (3) chemical oxidation with cerium (IV).

4.1.3.1 Electrolytic Decontamination

Electrolytic Decontamination

An electrolytic decontamination cell has been set up and testing with contaminated stainless steel plates was initiated. The plates are contaminated with a known quantity of ^{241}Am. Tests have been conducted at various temperatures and time intervals to determine the removal rate. Initial test results show that electropolishing does remove the contamination; however, the removal rate is relatively slow.

Chemical Extraction with the TechXtract Method

Testing with the TechXtract chemicals and radioactive-contaminated plates was started. Initial test results show that the TechXtract process effectively removed the ^{241}Am tracer (>99% removal). The treatment process required a lot of manipulations (i.e., moving the plate from one solution to another). The manufacturer was requested to recommend an alternative procedure to reduce the number of manipulations. Testing with the alternative procedure is in progress.

Chemical Oxidation with Cerium (IV)

Testing with cerium (IV) nitrate and radioactive-contaminated tracer plates was started. Tests have been conducted by varying solution temperature and immersion times. The results show that the ^{241}Am was effectively removed from the plates (>99% removal).

Chemical Treatment with Nitric Acid

This treatment was added after seeing the success of the cerium (IV) nitrate. It was decided to determine how much of the contamination could be removed without the cerium (IV) component. Testing has been conducted by varying solution temperature and immersion times, similar to the cerium (IV) testing. The initial test results show that the nitric acid (0.5 M) was more effective when the solution temperature was warm, but not quite as effective as the cerium (IV) nitrate. A preliminary assessment is that it may be reasonable to use the 0.5 M nitric acid as a first step to decontaminating items and then perhaps using one of the other treatment steps to further decontaminate the items. Further testing with items that are more representative of envisioned contaminated hardware will determine if this is a realistic approach.

Once the results of the small plate decontamination effort have been compiled and reviewed, we will begin testing more difficult materials using the successful treatment methods.

4.2 CONCEPTUAL PLANNING

4.2.1 Conceptual Design Studies

We have begun to identify items of equipment that can be improved to yield more reliable processing and/or reduced waste generation. Our plan is to focus on items that may be troublesome to repair and seek better methods of accomplishing the functions carried out by those items. To date, we have identified the off-gas scrubber, air operated control valves, and pumps for analysis.

We have also begun vendor surveys to identify off-the-shelf components that are either usable as is or may require slight modifications. We have identified another source for an off-gas scrubber and are pursuing additional information.

INTERNAL DISTRIBUTION

1. E. P. George
2. J. S. Ivey
3. J. F. King
4. C. G. McKamey
5-7. J. P. Moore
8. E. K. Ohriner
9. G. R. Romanoski
10. G. B. Ulrich
11. M. C. Vance
12. R. M. Wham
13. Laboratory Records

EXTERNAL DISTRIBUTION

14-24. U. S. DEPARTMENT OF ENERGY, NE-50, Germantown Building, 11901 Germantown Road, Germantown, MD 20874-1290

W. J. Barnett
C. E. Brown
J. Dowicki
L. W. Edgerly
R. R. Furlong
L. C. Herrera
A. S. Mehner
W. D. Owings
R. C. Raczynski
L. L. Rutger
E. J. Wahlquist

25. DEPARTMENT OF ENERGY, Albuquerque Field Office, P.O. Box 5400, Albuquerque, NM 87115

R. L. Holton

26-27. DEPARTMENT OF ENERGY, Oak Ridge Operations Office, Bldg. 4500N, Oak Ridge, TN 37831

L. W. Boyd, Mail Stop 6390
S. R. Martin, Jr., Mail Stop 6269

28. DEPARTMENT OF ENERGY, Los Alamos Area Office, 528 35th Street, Los Alamos, NM 87544

R. J. Valdez

29. DEPARTMENT OF ENERGY, Savannah River Operations Office, Bldg. 703F, P.O. Box A, Aiken, SC 29802

S. W. McAlhaney

30. DEPARTMENT OF ENERGY, Miamisburg Office, P.O. Box 66, Miamisburg, OH 45342

T. A. Frazier

31-32. BABCOCK AND WILCOX OF OHIO, INC., 1 Mound Road, Miamisburg, OH 45343-3000

D. M. Gabriel
J. R. McDougal

33-34. LOCKHEED MARTIN ASTRONAUTICS, P.O. Box 8555, Philadelphia, PA 19101

R. J. Hemler
R. M. Reinstrom

35. LOS ALAMOS NATIONAL LABORATORY, P.O. Box 1663, NMT-9, MS E502, Los Alamos, NM 87545

E. M. Foltyn

36. TETRA TECH NUS INC., 910 Clopper Road, Suite 400 Gaithersburg, MD 20878-1399

B. W. Bartram

37-38. ORBITAL SCIENCES CORPORATION, INC., 20301 Century Blvd., Germantown, MD 20874

R. T. Carpenter
E. A. Skrabek

39. PHILLIPS LABORATORY, Kirtland Air Force Base, AFRL/VSDV, 3550 Aberdeen Avenue SE, NM 87117

C. Mayberry

40. TELEDYNE BROWN ENGINEERING-ENERGY SYSTEMS, 10707 Gilroy Road, Hunt Valley, MD 21031

M. F. McKittrick

41. TEXAS A&M UNIVERSITY, Center for Space Power, Mail Stop 3118, College Station, TX 77843

M. J. Schuller

42. WESTINGHOUSE ADVANCED TECHNOLOGY BUSINESS AREA, P.O. Box 355, Pittsburgh, PA 15230-0355

M. O. Smith

43. WESTINGHOUSE SAVANNAH RIVER COMPANY, Savannah River Site, Aiken, SC 29808

R. W. Saylor